Section 2
PROGRESS IN LASER FUSION

2.A Absorption-Lines Measurement of Tamper $\rho\Delta R$ in Laser-Imploded Targets

Laser-imploded targets, especially those imploded adiabatically, attain high temperatures in the compressed core. The imploded part of the surrounding tamper is considerably colder, especially if preheat is small. Under these conditions the continuous x-ray emission from the core undergoes absorption at wavelengths characteristic of atomic species in the tamper. The resulting absorption lines can yield information on the temperature (T_e), density (ρ), and the $\rho\Delta R$ product of the tamper (density times thickness). Absorption can be particularly strong on resonance lines of the type 1s-2p in ions that have one or more vacancies in the n = 2 shell. The optimal choice of tamper species for this method is such that at the prevailing tamper temperature, ionization will remove some of the n = 2 electrons as well as all electrons of higher shells. For the present experiment, chlorine was a good choice, and, therefore, a KCℓ absorption layer was embedded within the tamper. Chlorine and potassium lines were observed and used to determine the conditions within the KCℓ layer and, by inference, within the rest of the tamper.

The experiment described here was performed on HELIOS, the eight-beam CO_2 laser system at the Los Alamos National Laboratory (LANL). The results were analyzed jointly by scientists from LANL and LLE. The typical target in this experiment consisted of a 350-μm-diameter glass shell of 0.8-μm thickness, coated with a 0.5-μm layer of KCℓ and then a 40-μm layer of CH. The fill gas was 15 atm DT and 0.2 atm Ar (approximately 10% Ar by mass or by total number of electrons). The severe electron preheat was mitigated by choosing a very thick tamper,
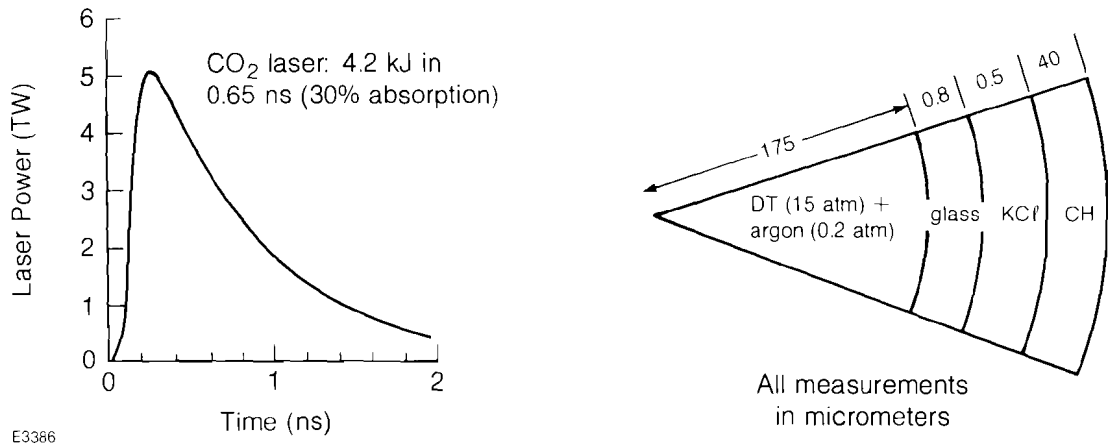
leading to modest preheat temperature. The tamper, after decompression from the preheat, recompresses to modest ρ and $\rho\Delta R$ values. It is then that very distinct absorption lines (of Cℓ and K) appear in the spectrum. The Ar doping causes a relatively small perturbation on the target behavior but provides a signature for core temperature diagnosis. In addition, it contributes to the continuum intensity in the range 2.5 – 3.5 keV, which is required to see Cℓ and K absorption lines.

The method of using tamper absorption lines was previously reported by LLE[1] and by LANL.[2] The Rutherford Laboratory[3] reported on similar observations in planar targets. We discuss below the advantages of using absorption of higher-Z ions and analyze the results in much more detail than has been previously done. The values of T_e and $\rho\Delta R$ derived from the experiment are in fair agreement with those predicted by the *LASNEX* laser-fusion code at LANL.

The absorption-lines method is similar to the method of neutron activation of tamper nuclei (such as ^{28}Si) except that here the temperature of the tamper can be determined as well. Furthermore, the method can be extended by using an external continuum source (in the backlighting mode). In this case, the parameters of the fuel can also be determined if a high-Z dopant is used. More important, the method can then be applied even if the core is too cold to emit x rays strongly.

We show in Fig. 22.1 the target and laser parameters used in this experiment. The very thick plastic coating is designed to yield a relatively low preheat temperature for the high total-preheat energy. For high enough total laser power, such a thick-shell target can still yield sufficiently high-core temperature to excite intense x-ray continuum around 3 keV (as well as 3- to 4-keV argon lines), which is a prerequisite for observing chlorine absorption lines. The relative position of the embedded KCℓ layer within the target is such that by the time of peak compression most or all of the CH layer (but none of the KCℓ layer) has been ablated. In order to relate the experimentally determined $\rho\Delta R$ of

Fig. 22.1
Target and laser parameters.

CO$_2$ laser: 4.2 kJ in 0.65 ns (30% absorption)

DT (15 atm) + argon (0.2 atm)

glass KCℓ CH

0.8 0.5 40

175

All measurements in micrometers

E3386

the KCℓ layer to that of the total tamper, we need to rely on code calculations. To minimize dependence on such calculations, the glass shell should be much thinner than the KCℓ layer. Alternatively, the $\rho\Delta R$ of the compressed glass shell should be determined independently from absorption lines of silicon (or calcium), and this was not done here.

Fig. 22.2(a) shows an example of the spectrum recorded on film using a PET diffracting crystal. Clearly seen are Ar emission lines as well as Cℓ and K absorption lines. The spatially resolving slit is too wide (40 μm) to show the size or structure of the core and is used here mainly to reduce detected emission from the target periphery, which does not participate in absorption-lines formation.

Fig. 22.2(b) shows a microdensitometer trace of the spatially resolved spectrum of Fig. 22.2(a). The background level lies just below the deepest absorption lines of Cℓ and K. This means that at the frequencies of peak absorption most of the photons emitted by the core are absorbed — i.e., the optical depth there is significantly larger than 1. There are two recombination continua: one (below about 5 Å) due to recombination of Si^{+14} ions; the other (below about 3.2 Å) due to recombination of Ar^{+17} ions. The slope of either of these continua corresponds to a temperature of about 700 eV. The Ar line-intensity ratio (1s – 2p)/($1s^2$ – 1s3p) can also be used to estimate the core temperature, and it yields ~600 eV; this ratio is chosen to avoid the large opacity of the $1s^2$ – 1s2p line. The contrast between strong Ar emission lines and strong Cℓ absorption lines vividly demonstrates a hot compressed core surrounded by a cooler shell. The tamper temperature deduced below is in fact much lower than this core temperature. The K lines appear less distinct than the Cℓ lines only because they are absorbed by a weaker continuum, and are therefore not analyzed in detail here. However, the absorption fractions on these lines and therefore the deduced $\rho\Delta R$ value are comparable to those of the Cℓ lines.

Figure 22.3 shows in more detail the Cℓ absorption structure. The identification of these lines was made by comparison with Hartree-Fock atomic structure calculations. As an example, the line marked B corresponds to transitions 1s – 2p in boron-like chlorine (Cl^{+12}) — i.e., $1s^2 2s^2 2p$ – $1s 2s^2 2p^2$; we likewise refer to other lines as the Be or the C feature, etc. For each configuration there can be several or many atomic states. For example, the He and Be features contain only one transition (ignoring a second, forbidden transition), whereas the B feature includes 14 transitions of which six are strong (i.e., gf is larger than 0.1); the C feature contains 35 transitions of which 12 are strong. The broadening of the B, C, and especially the N, O features is to a large extent due to the splitting between the lines comprising each manifold (which are blended because of additional broadening). For example, the measured width of the B feature is about 14 eV, that of the Be feature 17 eV. The widths due to line splitting of, for instance, the B and N features are 6 and 12 eV, respectively. The Be feature has no such broadening.

The remaining broadening mechanisms affecting these features are instrumental broadening (about 3 eV) and Stark broadening. Additionally, the results below indicate that the optical depth at the peak of the
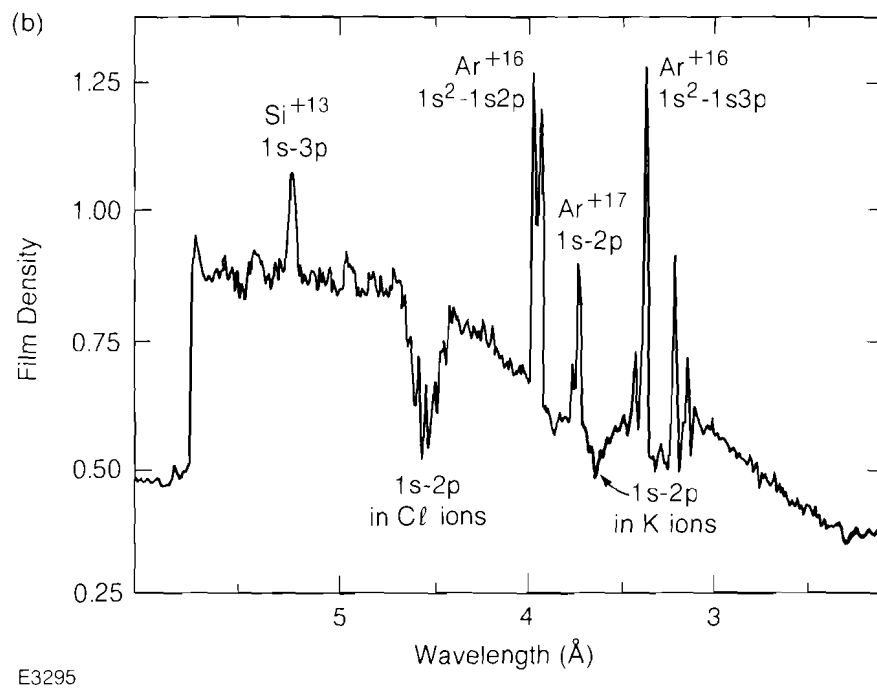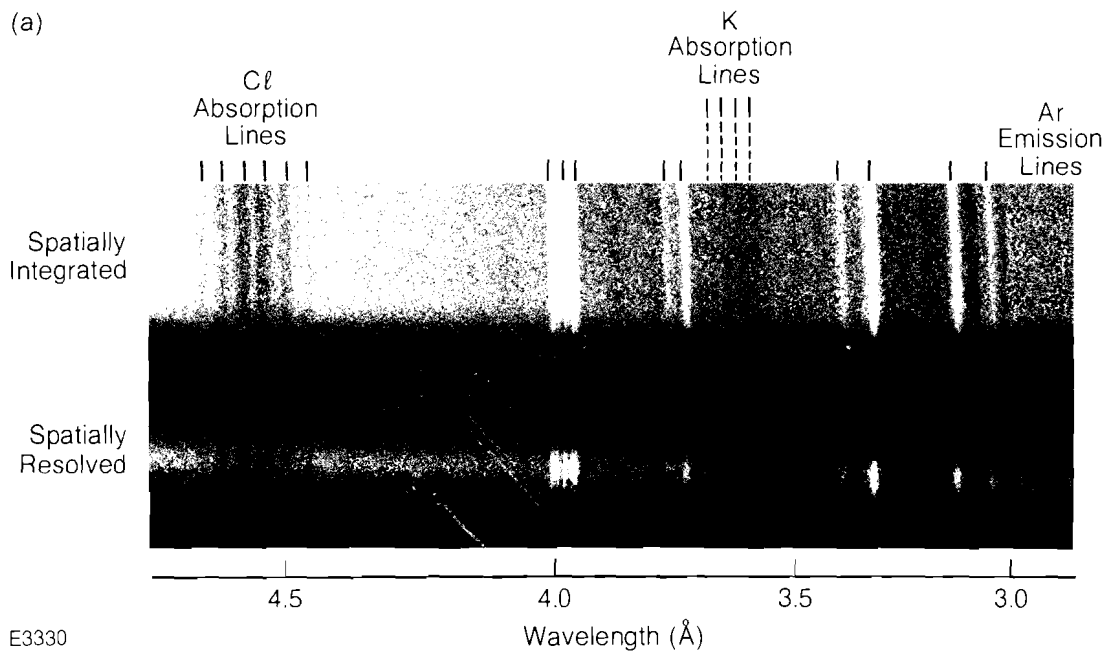
(a)

Cℓ
Absorption
Lines

K
Absorption
Lines

Ar
Emission
Lines

Spatially
Integrated

Spatially
Resolved

E3330

| | 4.5 | | 4.0 | | 3.5 | | 3.0 |

Wavelength (Å)

(b)

Film Density

1.25

1.00

0.75

0.50

0.25

Si^{+13}
1s-3p

Ar^{+16}
1s^2-1s2p

Ar^{+17}
1s-2p

Ar^{+16}
1s^2-1s3p

1s-2p
in Cℓ ions

1s-2p
in K ions

5   4   3

Wavelength (Å)

E3295

Fig. 22.2
(a) Film data obtained with a crystal x-ray spectrograph. White lines are emission lines of argon from the compressed core; black lines are absorption lines (of chlorine and potassium) from the tamper. (b) Microdensitometer tracing of the spatially resolved spectrum of (a) showing line identification.
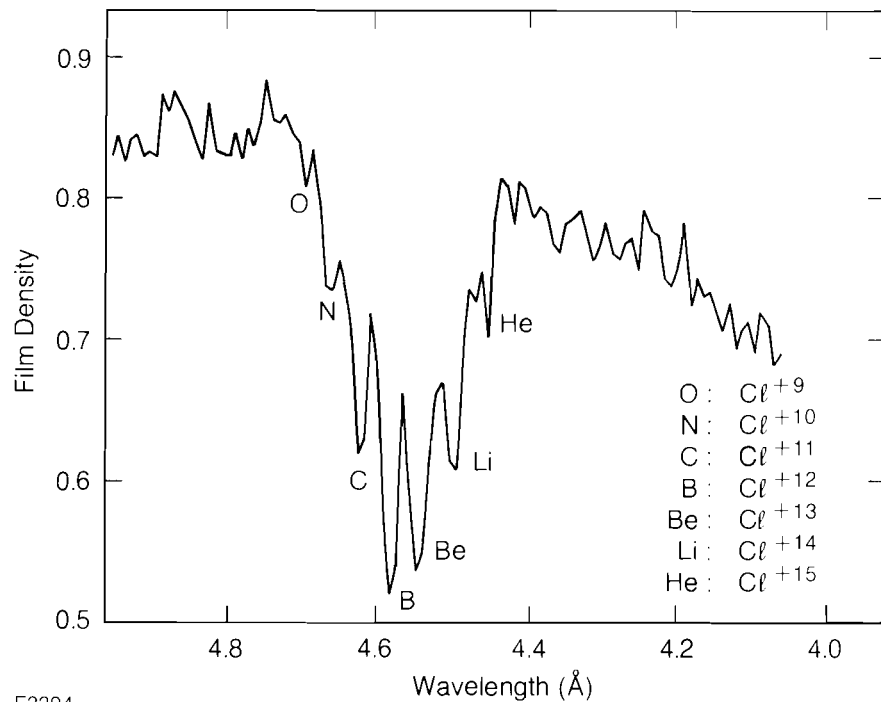
E3294

Fig. 22.3
Detailed tracing of the chlorine absorption
lines of Fig. 22.2(b). The feature marked B
corresponds to the transition 1s-2p in
boron-like chlorine (Cl^{+12}), etc.

Stark profile for these lines is much greater than 1 (the FWHM of the
Stark profile of those lines is estimated to be less than 1 eV for electron
density of the order 10^{23}cm^{-3}). Under these conditions the core radi-
ation at the peak of the profile is depleted. The absorption line then
broadens to a width such that the optical depth on the wings (e.g., the
half-intensity points) is of the order 1. The line widths then depend both
on ρ and $\rho\Delta R$ and, especially because of the unavailability of Stark
profile calculations for these lines, are not used here as diagnostic
signatures.

The tamper temperature at the time of strong continuum emission
from the core can be inferred from the intensity ratios of the absorption
features. At higher tamper temperatures than here, features such as He
or Li would dominate the absorption spectrum; at lower tamper
temperatures it would be features such as N and O. The fact that the
absorption features have a sharply peaked distribution of intensity is an
indication that they are formed over a period when the temperature
does not vary appreciably.

In order to estimate the tamper temperature from Fig. 22.3 we
calculate the steady-state distribution of Cl charge states in a model that
includes radiative, dielectronic, and three-body recombination, as well
as ionization. The results (Fig. 22.4) show that this distribution depends
primarily on the temperature and only slightly on the density in the
range 10^{23}–10^{24} cm^{-3}. For this density range the deduced tempera-
ture by comparison to Fig. 22.3 is in the range 200–230 eV. The width

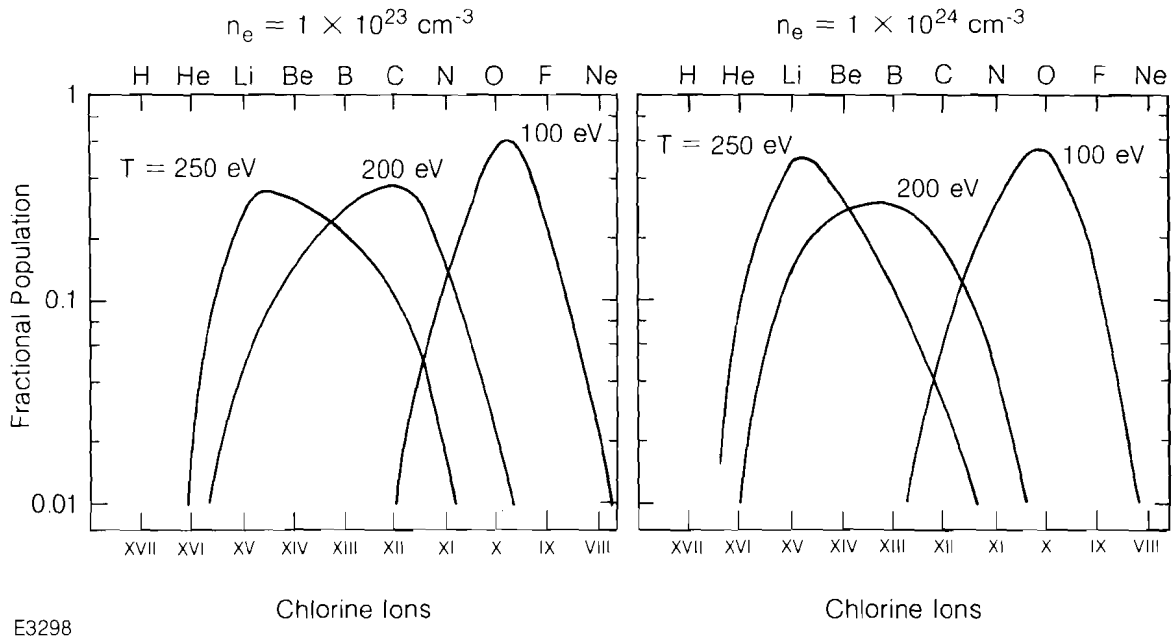$n_e = 1 \times 10^{23}$ cm^{-3} $n_e = 1 \times 10^{24}$ cm^{-3}

E3298

Fig. 22.4
Atomic model calculations of chlorine charge state distribution at two densities. Smooth lines connect the calculated discrete points. Comparison of such curves to the spectrum of Fig. 22.3 is used to estimate the tamper temperature.

of the experimental and calculated distributions is comparable, indicating a temperature which does not vary appreciably over the time when the absorption features are formed. The determination of the tamper temperature, therefore, is not degraded as a consequence of not resolving the spectrum in time.

The determination of the tamper $\rho\Delta R$ from the absorption lines is based on the cross section for photo-absorption on a spectral line of profile $I(\nu)$, normalized to total area of unity:

$$\sigma_\nu = (\pi e^2/mc)\, f\, I(\nu), \tag{1}$$

where f is the absorption oscillator strength.

The attenuated intensity $I(\nu)$ through a layer of thickness ΔR and density ρ is related to the incident intensity I_0 (assumed independent of frequency) through

$$I(\nu) = I_0 \exp(-\sigma_\nu N_i \Delta R) = I_0 \exp(-\sigma \alpha \rho \Delta R/M_i), \tag{2}$$

where α is the fraction of all ions of type i, which are in the ground state and whose density is N_i. For the case of absorption lines α is inevitably very nearly equal to 1 because the temperature where they are formed is much smaller than the excitation energy of these lines. For some of these chlorine ions the ground configuration consists of several closely spaced states, and their total population densities are added; this means that the f value in Eq. (1) has to be averaged over the lower-state levels as well as summed over the upper-state levels. For example, the Be ion

has one ground state (^1S_o); the B ions, two ($^2P_{1/2}$, $^2P_{3/2}$); and the C ion, five ($^1D_2$, ^1S_o, $^3P_2$, $^3P_1$, $^3P_0$).

The $\rho\Delta R$ can then be derived from the equation

$$\rho\Delta R = (M_i/\sigma\alpha) \int \ell n \, (I_o/I_\nu) \, d\nu. \qquad (3)$$

The integral is effectively over the line profile because the integrand vanishes far from line center. In the approximation that the film density in Fig. 22.3 is proportional to ℓn (I), this integral is simply the area enclosed within the absorption line. For each absorption line, this equation yields the partial $\rho\Delta R$ value related to the corresponding ion. The total $\rho\Delta R$ of the KCℓ layer is given by

$$\rho\Delta R \, (KC\ell) = 2.2 \; \rho\Delta R \; (C\ell) = 2.2 \sum_i \rho\Delta R \; (C\ell_i), \qquad (4)$$

where the summation is over the absorption-lines manifold in Fig. 22.3.

It is important to note that only the integral over the line profile is required for the determination of $\rho\Delta R$, so that the line profile need not be known. Also, the deconvolution required to separate the contribution of the partly overlapping absorption lines is not critical. For example, if the f values of these absorption lines were the same, we would only need to integrate the entire absorption manifold of Fig. 22.3 without any deconvolution.

Applying the procedure described here to the absorption lines of Fig. 22.3, following conversion from film density to intensity, overlapping lines deconvolution, and integration, we derive a value of

$$\rho\Delta R = 5.3 \times 10^{-4} \; g/cm^2$$

for the KCℓ layer. The main sources of error in deriving the $\rho\Delta R$ value come from the determination of the area enclosed within the absorption lines and from uncertainties in film calibration curves. These errors are estimated to be ±20%. An additional error in time-integrated spectra can be caused by core emission of continuum, prior to the time the absorption lines are formed. This can occur when the core starts to compress and heat up, but the shell still moves inward and is too cold to absorb on 1s-2p transitions because there are no vacancies in the n = 2 electronic shell. This error should in general be small because of the logarithmic dependence of the derived $\rho\Delta R$ value on the measured intensity [Eq. (3)]; it always results in underestimating the correct $\rho\Delta R$ value. If at least one of the absorption lines approaches the background level [as is the case for both the Cℓ and K groups in Fig. 22.2(b)], then this effect is unimportant and temporally resolving the spectrum is not essential.

The *LASNEX* laser-fusion code in a one-dimensional mode was used to simulate these experiments. In Fig. 22.5, we show the calculated time history of the electron temperature, averaged over each target layer. At the time of peak core temperature, which should be about the time of peak core emission of continuum, the temperature in the KCℓ layer is
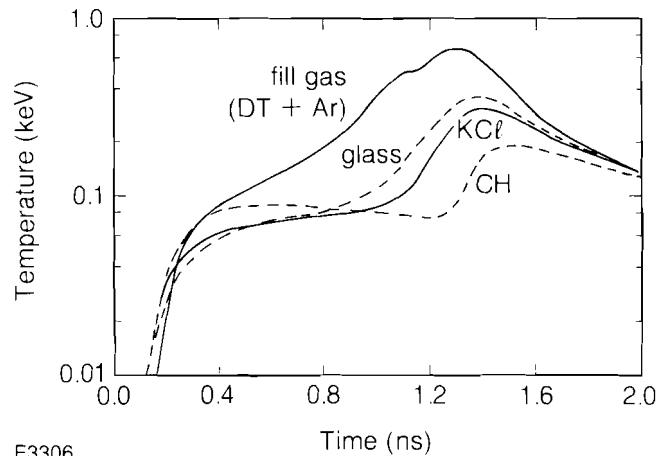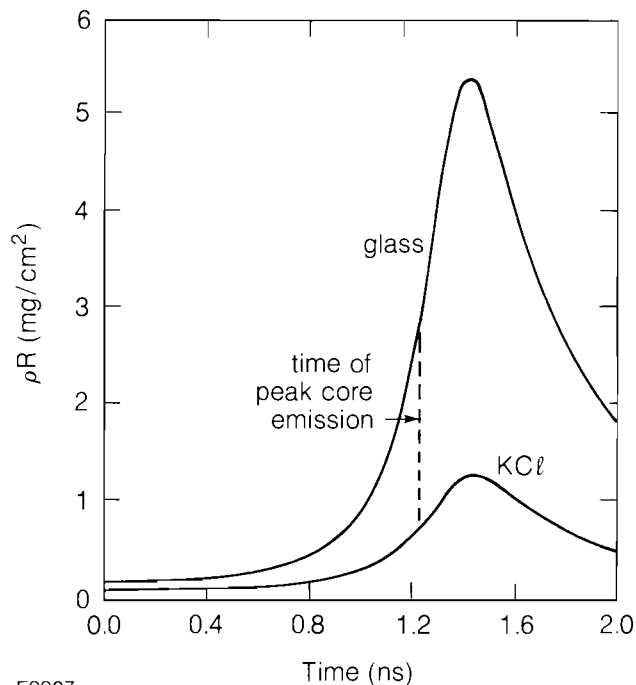
Fig. 22.5
LASNEX-calculated temperature history averaged over each of four target layers.

predicted to be 250 eV, in good agreement with the range 200–230 eV determined from the experiment. It should be pointed out that the predicted preheat temperature is only about 80 eV. The rise in tamper temperature, at about 1.1 ns, is due to heat flowing outward from the hot fill gas as well as due to the recompression of the expanded tamper. As is evident by comparing Figs. 22.1 and 22.5, the compression occurs much after the peak of the laser pulse.

Figure 22.6 shows the time history of the $\rho\Delta R$ of both the glass and KCℓ layers. At the time of peak core temperature, assumed to be the time of peak core emission, the $\rho\Delta R$ of the KCℓ layer is

$$6.8 \times 10^{-4} \text{ g/cm}^2,$$

in rough agreement with the experimentally derived value. We can infer from here by using the computational results of Fig. 22.6 that the total $\rho\Delta R$ of the tamper at that time was about 3.4×10^{-3} g/cm^2. An important conclusion from Figs. 22.5 and 22.6 is that this method is useful in determining the peak tamper $\rho\Delta R$ only if the implosion is well timed so that the peaks in core temperature and in tamper $\rho\Delta R$ occur at the same time. For future high-performance target implosions (such as expected with short-wavelength lasers), the target tamper in similar experiments will have to consist of a very thin signature layer in a low-Z (plastic) shell. This is because a high-$\rho\Delta R$, compressed shell can absorb strongly even photons of nonresonant frequency (by the photo-electric, or bound-free, mechanism) so that no absorption lines would appear in the spectrum. This problem will be especially severe in such targets because the tamper temperature is expected to be lower, which will necessitate choosing a lower-Z signature layer. Otherwise, no electrons of the $n = 2$ shell will be ionized. Lower-Z ions have transitions of longer wavelength where the absorption is even more severe. To counter such excessive absorption, the targets should have a thin enough signature layer, located deep enough in a low-Z tamper, so that it does not undergo ablation or expansion before peak compression of

Fig. 22.6
LASNEX-*calculated* $\rho\Delta R$ *history for the two tamper layers.*

E3307

the core. The choice of chlorine for the present experiment was appropriate because for higher-Z species (even for potassium) the lower-continuum intensity limits the precision; on the other hand, for much lower-Z species, the glass-shell absorption is severe even in the present experiment. A more detailed determination of tamper parameters can be obtained by embedding several signature layers within the inner part of the tamper with deeper layers having a higher nuclear charge-Z species.

ACKNOWLEDGMENT

REFERENCES

1. B. Yaakobi, R. L. McCrory, S. Skupsky, J. A. Delettrez, P. Bourke, H. Deckman, C. F. Hooper, and J. M. Soures, *Opt. Commun.* **34**, 213 (1980).

2. A. Hauer, in *Spectral Line Shapes*, edited by B. Wende (Springer, Berlin, 1981).

3. D. K. Bradely, J. D. Hares, and J. D. Kilkenny, Rutherford-Appleton Laboratory Annual Report RL-83-043, p. 5.4.